Appl. Phys. A 65, 535–542 (1997)

Applied Physics A Materials Science & Processing



# (e,2e) electron spectroscopy of surfaces

**O.M. Artamonov, S.N. Samarin, J. Kirschner**

Max-Planck-Institut für Mikrostrukturphysik, Weinberg 2, D-06120 Halle, Germany
(Fax: +49-345/5511-223; E-mail: artaman@mpi-halle.mpg.de, samar@mpi-halle.mpg.de)

Received: 21 March 1997/Accepted 12 August 1997

**Abstract.** In (e,2e) spectroscopy, a primary electron is scattered from a target and detected in coincidence with another electron ejected from the target. We measured such events in electron scattering from a W(100) surface by two time-of-flight electron energy analyzers based on position sensitive multi-channel detectors. We analyzed the total energy distribution of correlated electron pairs, as well as the energy-sharing distributions of electrons within a pair with a certain total energy. We found that the correlated electron pairs are created mainly by the primary electron scattering off a valence electron close to the Fermi level. An asymmetry in the energy-sharing distributions of the electrons of the correlated pair appears when the incident electron direction is off-normal. We suggest that most of the correlated pairs from W(100) are created by the specularly reflected or diffracted primary electrons and are due to a single scattering event of the primary electron with a valence electron.

**PACS:** 73.20.At; 79.20.-m

In conventional electron spectroscopy, with excitation by electrons or photons, we generally observe an integral response of the electronic system of the solid to an external excitation. There is very little information about individual electron-electron scattering events in solids. To obtain such information is difficult, both experimentally and theoretically. Experimentally, it is difficult to separate single scattering events from multiscattering processes, as well as from collective excitations of the electron charge density (e.g., plasmon). The theoretical calculation of the scattering event requires two initial and two final electron states to be calculated with a largely unknown interaction potential.

One of the most promising techniques to study electron-electron scattering is two-electron coincidence spectroscopy in the mode of one electron in-two electrons out (e,2e spectroscopy) [1,2]. Over the last twenty years, (e,2e) spectroscopy has developed as a tool for studying the electronic structure of solids and scattering dynamics of fast electrons on solid targets [1–6]. All these studies were carried out in the transmission mode of (e-2e) experiments by using high-energy incident electrons. A fast electron knocks out a target electron and then scattered and ejected electrons are detected in coincidence. In this geometry, the scattering problem is kinematically complete: energy $E_0$ and momentum $\boldsymbol{k}_0$ of the incident electron are known, and energies $E_1$, $E_2$ and momenta $\boldsymbol{k}_1, \boldsymbol{k}_2$ of both time-correlated electrons are measured. One can obtain the binding energy $E_b$ and momentum $\boldsymbol{k}_v$ of the target electron by using energy and momentum conservation laws:

$$E_b = E_0 - E_1 - E_2 , \tag{1}$$

$$\boldsymbol{k}_v = \boldsymbol{k}_1 + \boldsymbol{k}_2 - \boldsymbol{k}_0 . \tag{2}$$

The data obtained with this mode of (e,2e) experiments concern the bulk electronic structure of a solid in the shape of a film, thin enough to transmit sufficient electrons and to justify the assumption of a single collision event.

In order to apply this technique to solid surfaces and to the study of the scattering dynamics of low-energy electrons, (e,2e) experiments in reflection geometry were designed [7–10]. In this mode, an incident electron impinges on the sample surface and two outgoing electrons are detected in coincidence. Two different modes were used in the reflection geometry experiments: (1) normal incidence and low primary electron energy [7–9] and (2) grazing angle of incidence and medium electron energy [10]. We shall focus our attention on experiments with low-energy primary electrons. In the case of the reflection geometry of the experiments, the momentum $\boldsymbol{k}_0$ of the incident electron is directed from vacuum to the solid, while the total momentum $\boldsymbol{k}_{tot}$ of two outgoing electrons is directed from the solid to vacuum. Thus, to describe the ionization in the reflection mode, further interactions that result in momentum reversal in addition to the electron-electron collision have to be considered. There are at least three models that describe additional elastic scattering. In the first model, the momentum normal to the surface is provided by the crystal that reflects the incident electron along the specular direction. In principle, not only the (0, 0) specular beam but all diffracted beams in the back hemisphere should be consid-

Invited paper presented at the DPG-Frühjahrstagung, Münster, Spring 1997.

ered. Their contribution to the number of observable (e,2e) events in the reflection mode depends on the arrangement of the experiment. In the second model, the incident electrons are isotropically scattered by the ion cores; some of them are turned around toward the surface and may create correlated electron pairs with the total momentum pointing toward vacuum. The third process, i.e., pair creation before diffraction, seems equally probable at first sight. However, after this event two electrons are traveling further into the crystal and two (independent) diffraction events are needed to redirect them toward the surface. This process is much less probable than the other two. Therefore, we focus on the elastic backscattering of the primary electron before the electron-electron collision.

This step is an important part of the process because it is the information about the primary electron momentum in the precollision state that gives us a chance to solve completely the scattering problem. The main goal of this work is to estimate the relative contribution of diffracted primary electrons (model 1) as well as of isotropically scattered primary electrons (model 2) to the creation of the correlated electron pairs.

We carried out the experiment in two different geometrical arrangements. In the first one, we investigated the contribution of specularly reflected primary electrons to the pair creation. For this we have used normal and small off-normal incidence angles of the primary electron beam. In the second arrangement, we estimated a possible contribution of diffracted primary electrons to the creation of correlated pairs. In the latter case we have used a grazing angle of incidence in order to avoid the correlated pairs generation by the specularly reflected beam. By changing the primary electron energy, we change the angle of the diffracted beam (beams) relative to the surface normal and detectors positions.

## 1 Experiment

Experiments were carried out in a μ-metal chamber with vacuum in the range of $10^{-10}$–$10^{-11}$ mbar. The W(100) crystal was mounted on a rotable holder. The sample cleaning procedure included oxidation of the sample, followed by high-temperature flashes to remove carbon from the sample surface. The cleanliness of the surface was monitored by Auger electron spectroscopy. We used two 75 mm MCP-based position sensitive electron detectors. The detectors and the electron gun were in the same plane that contained the sample surface normal. In the case of normal and off-normal incidence, the detectors were placed in a symmetric position at ±40° with respect to the electron gun axis. The angle between the detectors was 80° in all cases. For the grazing incidence geometry, another position of the electron gun was used, i.e., rotated away from the previous direction by 95°. The distance $L$ between the sample and detectors can be varied within the limits of 130–263 mm. The position sensitive detectors allowed us to control the electron beam position on the sample by observing the specular beam as well as the diffracted beams. We combined coincidence and time-of-flight techniques to measure simultaneously the energies and momenta of both scattered electrons.

Our experimental set-up is shown in Fig. 1. An incident electron current of the order of $10^{-14}$ A, on average, was

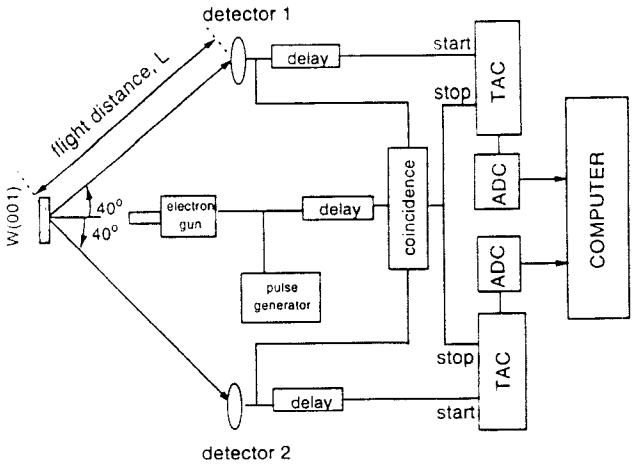


Fig. 1. Experimental set-up of the (e-2e) time-of-flight spectrometer. ADC, Analog-to-Digital Converter; TAC, Time-to-Amplitude Converter. Detectors 1 and 2 are based on 75 mm diameter multi-channel plates with resistive anode. $L$ is equal to $13 \div 26$ cm. The pulse generator pulses the primary electron current (pulse width is about 1 ns) and synchronizes the time scales of the TAC

pulsed with a width of about 1 ns and a repetition rate of $2.5 \times 10^6$ pulses per second. The trigger pulse from the generator was used as a reference point on the time-of-flight scale. When the incident electron generates a correlated pair of electrons and they are detected by the detectors, the two pulses start two time-to-amplitude converters (TAC). The stop pulse to both TAC comes from a logic unit that delivers a pulse only when the two delayed and shaped pulses from the detectors and the delayed trigger pulse from the generator coincide within a time window of 200 ns. A valid event represents a point in a two-dimensional time-of-flight coordinate system. One of the coordinates of this point defines the time of flight of the first electron of the pair and the second coordinate defines the time of flight of the second electron of the pair.

The principle of the time-of-flight electron energy measurement is simple. One measures the time of flight $\Delta T$ of the electron over the known distance $\Delta L$ (in a field-free space) between the sample and the detector. Then the kinetic (flight) energy of the electron is

$$E = \frac{m}{2}\left(\frac{\Delta L}{\Delta T}\right)^2 . \tag{3}$$

where $m$ is the electron rest mass.

From (3), it is clear that we measure the kinetic energy of electrons by their flight time. We measured more precisely the kinetic energy $E_p$ of the primary electron on the base of (3) by measuring the relative time of flight of elastically scattered electrons $\Delta T$ for different distance of flight $\Delta L = L_1 - L_2$. After that, we used the measured energy $E_p$ of the primary electron as a reference to calibrate the energy scale of the time-of-flight analyzers. Indeed, the zero point in Fig. 2a corresponds to the arrival time of an incident electron elastically reflected from the sample. Any other point on the time scale denotes the flight time $T$ of a slower electron. This time $T$ is measured with respect to the arrival time of the electron

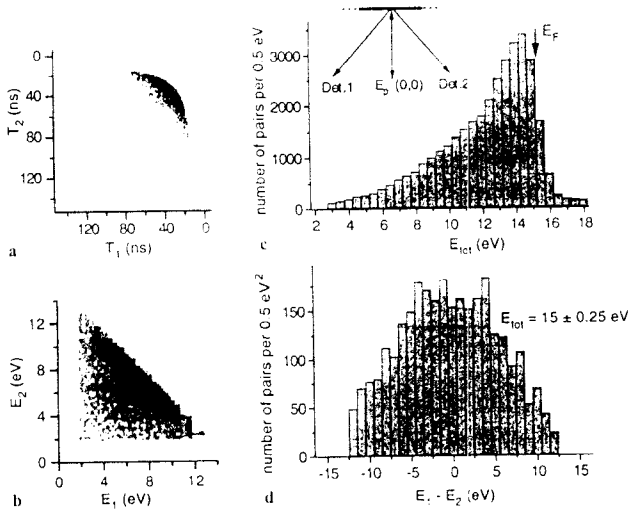


**Fig. 2a–d.** Time-of-flight and energy distributions of correlated electron pairs for normal incidence. $E_p = 20$ eV. $T_1$ and $T_2$ are the times-of-flight and $E_1$ and $E_2$ are the energies of scattered electrons. The distributions of coincidence events are displayed on a two-dimensional gray scale plot, black being the highest number of events. **a** Two-dimensional time-of-flight distribution of correlated pairs. **b** Two-dimensional energy distribution of correlated pairs. **c** Histogram of the correlated pair distribution as a function of the total energy of the pair. The height of the column represents the number of events (per 0.5 eV) within the total energy band $E_{tot} \pm 0.25$ eV. **d** Energy-sharing distribution of correlated pairs. The height of the column represents the number of pairs (per 0.5 eV$^2$) with the energy difference $E_1 - E_2$ within the total energy band $E_{tot} = 15 \pm 0.25$ eV

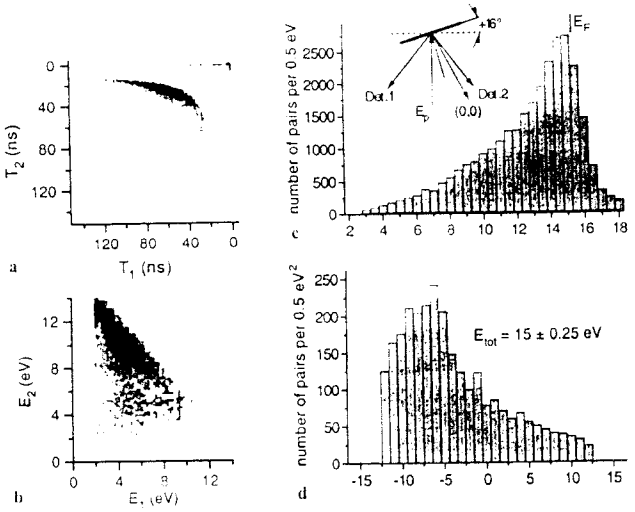


**Fig. 3.** Time-of-flight and energy distributions of correlated electron pairs for off-normal incidence. $E_p = 20$ eV, angle of incidence $\alpha = 16°$. **a–d** have the same meaning as in Fig. 2. In contrast to Fig. 2 the time-of-flight distribution, the two-dimensional energy distribution and the energy-sharing distribution are asymmetric

with the primary energy $E_p$. That is,

$$T = L\left(\sqrt{\frac{m}{2E}} - \sqrt{\frac{m}{2E_p}}\right), \tag{4}$$

where $L$ is the distance between the sample and the detector. Solving (4), we have

$$E = \frac{m}{2}\left(\frac{T}{L} + \sqrt{\frac{m}{2E_p}}\right)^{-2} \tag{5}$$

We can convert a time-of-flight scale $T$ to an energy scale $E$ by using (5).

## 2 Experimental results

Three two-dimensional time-of-flight distributions of correlated electron pairs are shown in Figs. 2a, 3a, and 4a. In Fig. 2 the direction of the primary electron is normal to the surface (normal incidence) and in Figs. 3 and 4, it has an angle ±16° relative to the surface normal in the detectors plane (off-normal incidence). The coincidence events are displayed in a two-dimensional gray scale plot, black being the highest number of events. The horizontal line and vertical line at the upper right corner of Figs. 2a, 3a, and 4a are due to accidental coincidences involving an elastically backscattered primary electron in the one detector and an inelastically scattered electron in the other detector. Their crossing is used to define the zero of the two time-of-flight scales. The ratio $N_t/N_a$ between the number of true coincidence events $N_t$ and the number of accidental events $N_a$ increases with decreasing incident electron current $I$, because $N_t \sim I$ and $N_a \sim I^2$.

A ridge-like maximum in these pictures represents the most probable combinations of electron energies within correlated electron pairs. In the case of normal incidence (Fig. 2a), the time-of-flight distribution is symmetric relative to the diagonal, while in the case of off-normal incidence (Figs. 3a, 4a), the time-of-flight distributions are asymmetric relative to the diagonal.

In Figs. 2b, 3b, and 4b the time-of-flight distributions are converted to energy distributions. The coincidence events are displayed in a two-dimensional gray scale plot, black being the largest number of events. The fine mesh in Figs. 2b, 3b, and 4b reflects the unit cell of the acquisition matrix with

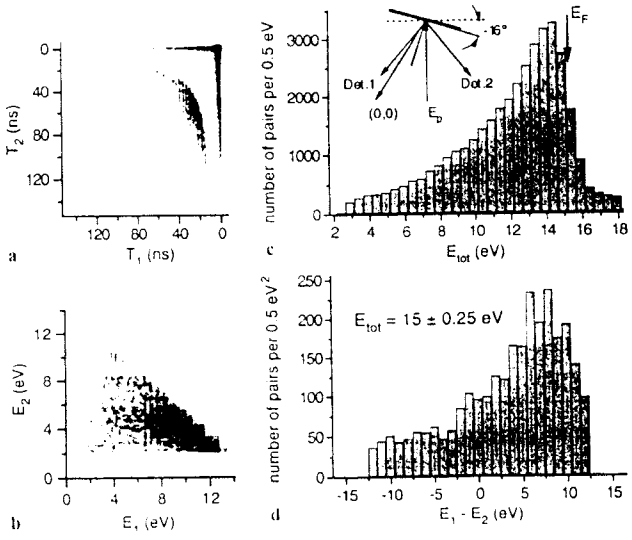


**Fig. 4.** Time-of-flight and energy distributions of correlated electron pairs for off-normal incidence. $E_p = 20$ eV, angle of incidence $\alpha = -16°$. **a–d** have the same meaning as in Fig. 2. In contrast to Fig. 2 the time-of-flight distribution, the two-dimensional energy distribution and the energy-sharing distribution are asymmetric. The asymmetry is reversed with respect to Fig. 3 (where $\alpha = 16°$)

the size of 1.6 ns × 1.6 ns. Our limited coincidence time window sets a lower limit of 2 eV to the electron energy. The ridge-like maximum of the time-of-flight distribution is transformed into a band along the line $E_1 + E_2 = 14$–$15$ eV in the energy distribution. The line $E_1 + E_2 = E_{tot}$ is the locus of electron pairs with a constant sum of energies $E_{tot}$ (we call it the "total energy" of a pair).

The diagonal on the energy distribution is the locus of pairs with equal energies of both electrons $E_1$ and $E_2$. The energy distribution in Fig. 2b is symmetric relative to the diagonal, while the energy distributions in Figs. 3b and 4b are asymmetric in accordance with the time-of-flight distributions. One can see that the more probable pair location (black spots) corresponds to different energies of electrons of the pair: $E_1 \cong 4$ eV, $E_2 \cong 11$ eV in Fig. 3b and $E_1 \cong 11$ eV, $E_2 \cong 4$ eV in Fig. 4b.

Since the incident electron energy $E_p = 20$ eV is known, we can calculate the binding energy $E_b$ of the target electron for the total energy of the pair $E_{tot} = 14$–$15$ eV : $E_b = E_p - E_{tot} = 5$–$6$ eV. Taking into account that the work-function of W(001) is 4.6 eV, one sees that the target electron is excited from energy levels just below the Fermi level. The line defined as $E_{tot} = 20 - 4.6 = 15.4$ eV corresponds to the excitation from the Fermi level. In the two-dimensional energy distributions (Figs. 2b, 3b, 4b), there are no correlated pairs beyond this line. Further analysis of the energy distribution is made by calculating the number of events in a total energy band $E_{tot} \pm 0.25$ eV as a function of $E_{tot}$. The distribution of the number of correlated electron pairs as a function of the total energy of the pairs ("total energy distribution") is shown in Figs. 2c, 3c, and 4c. The maximum of these distributions is at $E_{tot} = 14$–$15$ eV, corresponding to electron excitation from energy levels below the Fermi level. It is remarkable that the shape of all these distributions is very similar, irrespective of the geometry. This is what one would expect for the isotropic model above, but it is even consistent with the backdiffraction model. Correlated electron pairs with lower total energies may originate either from the excitation of valence electrons from deeper energy levels or/and from inelastic scattering.

The energy-sharing distributions in Figs. 2d, 3d, and 4d represent the number of pairs with energy difference $E_{dif} = E_1 - E_2$ within the total energy band $E_{tot} = 15 \pm 0.25$ eV. One can see that the energy-sharing distribution in Fig. 2d (normal incidence of the primary electrons) is symmetric with respect to the energy $E_{dif} = 0$, where the energies of both correlated electrons are equal. The energy-sharing distribution for the off-normal incidence of the primary electrons (Figs. 3d, 4d) clearly shows that the most likely difference between the energies of the two electrons is ±7 eV. In both cases (Figs. 3d, 4d) the electron with the higher energy of the two is detected by the detector placed at a smaller angle to the surface normal. We note that in the energy-sharing distributions, the crystal orientation proves to be of importance, in contrast to the total energy distributions.

Figure 5a,b presents energy-sharing distributions of correlated pairs for $E_p = 20$ eV and three selected values of $E_{tot}$($E_{tot} = 15$, $E_{tot} = 11$, and $E_{tot} = 9$ eV); geometries of measurements are given in top panels of Fig. 5. The angle between the detectors is equal to 80° in both cases, but the surface normal is tilted by 16° to the detector 2 for Fig. 5b (positive polar angle) and by −16° to the detector 1 for Fig. 5a (negative polar angle). Energy-sharing distributions

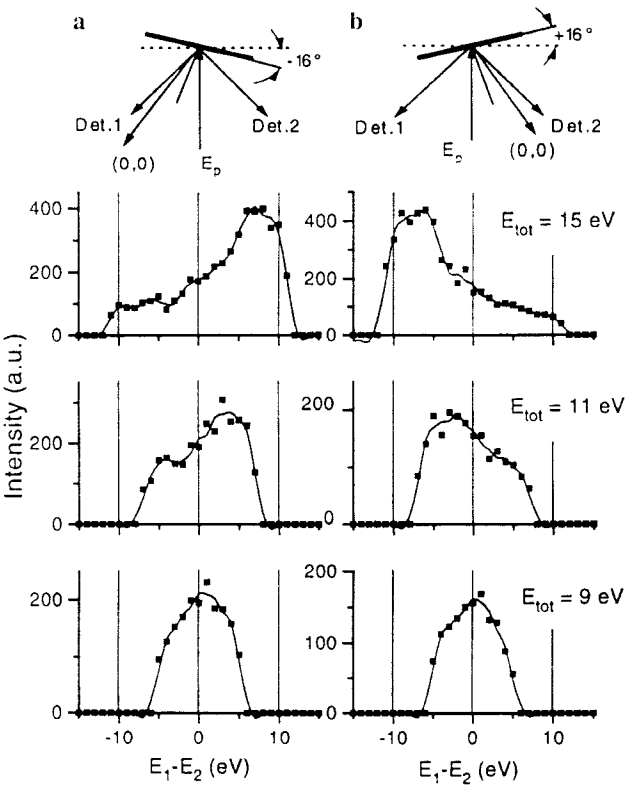


**Fig. 5a,b.** Energy-sharing distributions of correlated pairs excited by an off-normal incident electron beam for different total energies ($E_{tot} \pm 0.5$ eV) of pairs. **a** The sample tilted by −16°. **b** The sample tilted by +16°. Note the gradual change from strongly asymmetric distributions at high total energy to symmetric sharing distributions at low total energy

for the total energy $E_{tot} = 15$ eV (valence electron states are just below the Fermi level) are asymmetric with respect to the middle point at the energy $E_1 - E_2 = 0$. The position of the maximum in Fig. 5a is at +7 eV, while in Fig. 5b, it is at −7 eV. For the total energy $E_{tot} = 11$ eV, the asymmetry still exists in both panels, but the maximum is shifted to ±4 eV. For the total energy $E_{tot} = 9$ eV, the energy-sharing distributions are symmetric for both geometries of the experiment. These observations suggest that for the off-normal incident electrons, the asymmetric kinematics of the electron-electron scattering causes the asymmetry of the energy-sharing distributions of the correlated electrons. This is valid only for correlated pairs generated in a single-step process because the electron pairs resulting from a multi-step process "forget" about the asymmetry of the excitation. This single-step process takes place in the energy range of valence electron energies 4 eV below the Fermi level ($E_{tot} = 11$–$15$ eV). The reason for the asymmetry in the energy sharing between the correlated electrons of the pair is the deviation of the direction of the specularly reflected primary electron from the bisector between the detectors. The electron with the higher energy of the two is scattered by a smaller angle. On the other hand, the symmetric energy-sharing distribution of pairs for $E_{tot} = 9$ eV (and lower) indicates that these pairs are most likely created in a multi-step process, possibly involving energy losses, in which the memory of the direction of the exciting primary beam got lost. The present observations lead to the conclusion that (at least for the single scattering process without inelastic energy loss) the cristallinity of the sample and the concomi-

tant diffraction effects play a major role. This means that we do not have an isotropic internal source of electrons traveling equally into all directions after an initial momentum change of the primary electron. In this case, rotating the target by $\pm 16°$ would not lead to a major asymmetry. On the contrary, we have to assume that we have a strongly anisotropic source with the primary beam directed along the specular direction, i.e., along the (0, 0) beam. Under conditions of strong multiple scattering, which we do have at the present low energies, a primary electron may be diffracted into higher-order beams with essentially the same probability.

This leads us to the following *Gedankenexperiment*: let us pass the primary electrons parallel to the surface of the crystal and adjust the energy such that a higher-order beam [say the $(-1, 0)$ beam] leaves the sample exactly along the surface normal. In this case the energy-sharing distribution should be symmetric with respect to zero energy difference and, moreover, the shape of the distribution should be exactly the same as if we used normally incident electrons of the same energy. This follows from time reversal symmetry in elastic scattering. If we now change the energy of the grazing incident beam by plus or minus a few eV, the diffracted $(-1, 0)$ beam will make a small negative or positive angle with the surface normal. As a consequence, the energy sharing distribution will become asymmetric with respect to zero energy difference. Unlike in the previous experiment, where we rotated the sample, the sharing distribution will not have the same shape but antisymmetric behavior, since we change the primary energy and hence change the excitation cross-section. However, for small energy changes, it will be approximately the same around zero energy difference. If there happens to be a peak of the sharing distribution at zero energy, this peak will move towards slightly negative or positive positions on the energy scale, depending on whether the diffracted $(-1, 0)$ beam includes a negative or positive angle with the surface normal.

Our *Gedankenexperiment* cannot be carried out in reality, of course, since we cannot make our beam exactly parallel to the surface. What we can do experimentally is shown in Fig. 6. The electron gun axis has an angle of 95° with respect to the bisector between the detectors and the sample normal is tilted by 7° relative to the bisector. As a result, the primary electron direction is about 2° relative to the surface plane or 88° relative to the surface normal. To verify the primary electron angle of incidence we measured the diffraction angle of the $(-2, 0)$ diffracted beam for 30 eV primary electrons with the position sensitive detector. The angle of the outgoing $(-1, 0)$ diffracted beam $\alpha_{1,0}$ relative to the surface normal is $\alpha_{1,0} = \arctan(k_{pt} - g_{10})/k_p$, where $k_p$ is the primary electron momentum, $k_{pt}$ is the tangential component of the primary electron momentum, and $g_{10}$ is the value of the reciprocal vector of the lattice ($g_{10} = 1.985\ \text{Å}^{-1}$). We did the (e,2e) experiment at this geometry for two different primary energies: 16.1 eV and 19.8 eV. It is easy to estimate that $\alpha_{1,0} = 2°$ for $E_p = 16.1$ eV and $\alpha_{1,0} = 7.4°$ for $E_p = 19.8$ eV. The experimental parameters for upper and lower panels of Fig. 6 differ by the energy of the primary electrons and by the direction of the primary electron diffraction. The direction of the $(-1, 0)$ diffracted beam at $E_p = 16.1$ eV (as we calculated earlier) is 2° relative to the surface normal or +5° relative to the bisector between detectors. When we increase the primary electron energy to $E_p = 19.8$ eV the angle of the $(-1, 0)$ diffracted

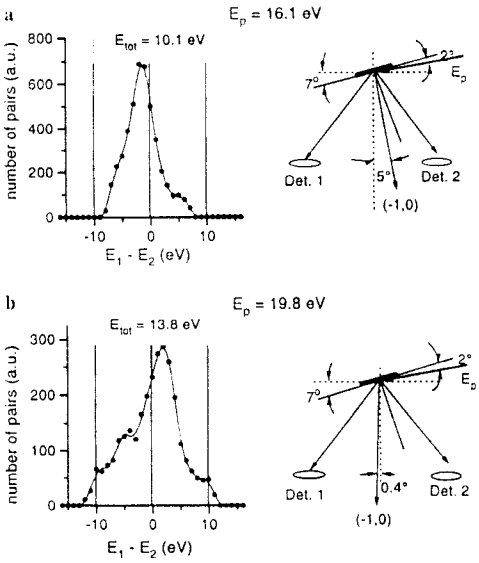


**Fig. 6a,b.** Energy-sharing distributions of correlated pairs for grazing incidence of the primary electron (2° relative to the surface plane). **a** $E_p = 16.1$ eV, $E_{tot} = 10.1$ eV. **b** $E_p = 19.8$ eV, $E_{tot} = 13.8$ eV. The position of the maximum shifts from −2 eV (**a**) to +2 eV (**b**) when one changes the direction of the $(-1, 0)$ beam (by changing the primary electron energy)

electron beam is shifted by 5.4° and it is −0.4° relative to the bisector.

For both primary electron energies we have well-defined maxima in the energy sharing distributions (Figs. 6a,b) in the energy band $E_{tot} \pm 0.5$ eV, and the widths of these maxima are relatively narrow. The total energy $E_{tot}$ in both cases was chosen at the same valence electron energies of $1.4 \pm 0.5$ eV below the Fermi level. The position of the peak in Fig. 6a is at $-2.5$ eV, while it is at $+3.3$ eV in Fig. 6b. This agrees nicely with our expectations from the Gedankenexperiment. The sharing distributions are not identical, since the two energies are different by 30% (hence, at least their widths must be different) but they are similar around the central peak. The shift toward opposite directions for the $(-1, 0)$ beam at +5° or −0.4° relative to the bisector between the detectors supports our conjecture that the electrons diffracted into a beam along the surface normal or its vicinity represent the main source of electrons for (e,2e) processes in the reflection geometry.

## 3 Discussion

In this section we consider how the experimental conditions restrict the volume in the $k$-space of the valence electrons, which can be studied by (e,2e) spectroscopy. In other words, which valence electron states can contribute (and which not) to the measured distributions of correlated pairs under given experimental conditions. On the basis of a simple model, we show that the asymmetry of the energy sharing distributions for off-normal incidence may originate from the asymmetry of the scattering kinematics. We conclude that for near normal incidence, correlated pairs are mostly generated by the specularly reflected beam, which may have some angle with the bisector of the angle between the detectors.

For the case of a single collision of the primary electron with a valence electron, we can easily calculate the energy

and momentum transfer ($\Delta E$ and $\Delta k$, respectively). We assume that the binding energy of the valence electron $E_b$ is identical to the energy transfer $\Delta E$:

$$E_b = \Delta E = E_0 - E_1 - E_2 . \tag{6}$$

The measured vector of the momentum transfer $\Delta k_{vac} = k_1 + k_2 - k_0$ relates to free electrons in vacuum (two scattered electrons and a primary one). We consider the scattering in the plane comprising the two detectors, the primary electron momentum direction, and the surface normal. $\Delta k_{vt}$ and $\Delta k_{vn}$ are the tangential and the normal components of the momentum transfer vector $\Delta k_{vac}$. From (2), we have

$$\Delta k_{vt} = \sqrt{2 \cdot E_1} \sin \vartheta_1 + \sqrt{2 \cdot E_2} \sin \vartheta_2 - \sqrt{2 \cdot E_0} \sin \alpha , \tag{7}$$

$$\Delta k_{vn} = \sqrt{2 \cdot E_1} \cos \vartheta_1 + \sqrt{2 \cdot E_2} \cos \vartheta_2 - \sqrt{2 \cdot E_0} \cos \alpha , \tag{8}$$

where $E_1$ and $E_2$ are the energies of the first and the second electron of the pair, and $\vartheta_1$ and $\vartheta_2$ are the angles between the detector directions and the surface normal. $E_0$ and $\alpha$ are the energy and the incident angle of the primary electron in vacuum (we used atomic units: $e = m = \hbar = 1$). To calculate the momentum of a valence electron one needs to take into account two effects. The first one is the change of the primary electron momentum during an elastic scattering. The second one is the change of the primary electron momentum and that of both scattered electrons by the surface potential barrier. Therefore, the momentum transfer vector inside the solid $\Delta k_s$ differs from the momentum transfer vector in vacuum. To calculate the momentum transfer vector inside the solid $\Delta k_s$, we used for simplicity only one parameter, the muffin-tin energy $E_{mt}$, to describe the solid. This means, that the kinetic electron energy in the solid will differ from the energy in vacuum by the value of $E_{mt}$. We assume the solid-vacuum boundary to be a plane, which leads to the conservation of the tangential component of the electron momentum: $\Delta k_{st} = \Delta k_{vt}$, where $\Delta k_{st}$ is the tangential component of the momentum transfer vector inside the solid. The normal component of the electron momentum is not conserved. One needs to know the dispersion relation for the electron in the solid $E(k)$ to calculate the change of the normal component of the electron momentum on the surface. We assume the primary electron and both scattered electrons in the solid to have a parabolic dispersion like a free electron. This assumption is widely used in photoelectron spectroscopy. Now the expression for the normal component of the momentum transfer $\Delta k_{sn}$ in the solid is

$$\Delta k_{sn} = \sqrt{2\left(E_1 \cos^2 \vartheta_1 + E_{mt}\right)} + \sqrt{2\left(E_2 \cos^2 \vartheta_2 + E_{mt}\right)} - \sqrt{2\left(E_0 \cos^2 \alpha + E_{mt}\right)} . \tag{9}$$

Within this simple model of the solid, we can link the measured momentum transfer with the valence electron momentum in the precollision state $k_v$:

$$k_v = \Delta k_s . \tag{10}$$

We did not use any limitation or assumption concerning the dispersion of the valence electron state of the solid and we can now scan the valence electron states by changing experimental parameters.

Let us now consider how the experimental parameters restrict the range of $\Delta k_s$ that can be measured. In general, the momentum transfer vector is a function of all kinematical parameters $\Delta k_s (E_1, E_2, \vartheta_1, \vartheta_2, E_p, \alpha)$. We expect, on the basis of experimental results, that the detected electron pairs are created mainly by the specularly reflected or diffracted primary electrons. Thus, the energy of the primary electron in the precollision state is $E_p$ and the direction of its momentum is defined by the specular reflection or diffraction conditions. The two-dimensional energy distribution in Fig. 2b has been measured at certain $E_p$, $\alpha$, $\vartheta_1$, and $\vartheta_2$ and it is a function of the two variables $E_1$ and $E_2$. To calculate the energy-sharing distribution, we have chosen $E_{tot} = 14$ eV and the energy-sharing distribution now is a function of only one variable $E_1$ or $E_{dif} = 2E_1 - E_{tot}$. From (7), (9), we can express $\Delta k_s$ as a function of $E_{dif}$ to be able to compare it directly with the experimental energy-sharing distributions. We can select the plane of scattering in the $k$-space of valence electrons. In our experimental geometry, the scattering plane coincides with the $\Gamma$-H plane of the W(100) crystal. Any value of $E_{dif}$ corresponds to a point in this scattering plane and the full range of $E_{dif}$ gives us a trace in the scattering plane. This trace is the locus of experimentally detectable states of the valence electrons. On the other side, we may select a certain binding energy of the valence electrons and all valence electron states in this selected energy region are on an equi-energy surface in $k$-space or on an equi-energy curve in the scattering plane. The intersection of the experimental scanning trace with the equi-energy curve in the scattering plane gives us in accordance with (10) the detectable valence electron states in the $k$-space of valence electrons.

Figure 7a,b,c presents three different scanning traces in the scattering plane in $k$-space (left hand panels) for various experimental geometries (right hand panels). The y-axes are the normal components of the momentum transfer vector

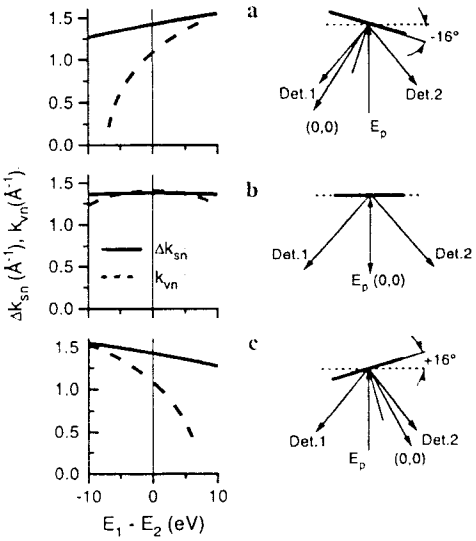


**Fig. 7a–c.** Calculated traces in $k$-space within the scattering plane. **a** The surface normal tilted by $-16°$, **b** normal incidence, **c** surface normal tilted by $+16°$. Plotted are the normal component of the momentum transfer vector $\Delta k_{vn}$ and the normal component of the valence electron momentum $-k_{fn}$ (in free-electron-like approximation) versus the energy difference $E_1 - E_2$. Solid lines are scanning traces in the scattering plane, dashed lines are the loci of the normal component of the valence electron momentum

$\Delta k_n$ and the normal components of a valence electron momentum $k_{vn}$. The x-axes represent $E_{dif}$ instead of $\Delta k_t$ to be comparable to the experimental curves. In all cases the primary electron beam is directed along the bisector between the detectors. Figure 7b corresponds to normal incidence of the primary electron, while the specularly reflected electron runs along the normal to the surface. In Fig. 7a the (0, 0) diffracted beam direction has the angle $-16°$ to the surface normal and in Fig. 7c the angle 16° to the surface normal. The solid lines in each left hand panel of Fig. 7 present the experimental scanning trace in $k$-space ($\Delta k_n$ versus $E_{dif}$). The traces (Fig. 7a,b) are tilted in agreement with the tilting of the (0, 0) diffracted beam. In contrast, in Fig. 7b the trace is symmetric relative to the middle point in agreement with the normal direction of the (0, 0) diffracted beam. The trace in the scattering plane gives us the locus of all electron states in $k$-space, which can be detected with the chosen experimental parameters. The real location of the $k_v$ point (points) on this trace depends on the shape of the equi-energy surface of valence electron states.

We can simulate the real equi-energy surface by the free-electron-like sphere to estimate the influence of experimental parameters on the restriction of valence electron states to be detected. We choose the energy of the free-electron-like valence electron $E_v = 10\,\text{eV}$, the momentum value is $k_v = (2E_v)^{1/2}$. We shall link the tangential component of the valence electron momentum with the tangential component of $\Delta k_s : k_{vt} = \Delta k_{st}$. The normal component of the valence electron momentum $k_{vn}$ is: $k_{vn} = (2E_v - k_{vt}^2)^{1/2}$. The dashed line in Fig. 7 (left-hand panels) presents the part of the valence electron equi-energy circumference in the $k_{vn}$ versus $E_{dif}$ coordinates. The crossing of the dashed lines with the solid lines in Fig. 7 defines in accordance with (10) the points of (or a region of) the actual location of the detectable electron states of the valence electrons with the energy close to the Fermi level. The location of these points depends on the geometry of the experiment. In the asymmetric geometry of the experiment defined on the right hand panels of Fig. 7a,c, one can detect the correlated pairs with unequal energies of correlated electrons. By contrast, only pairs with approximately equal energies of electrons can be detected in the symmetric geometry of the experiment defined on the right hand panel of Fig. 7b.

One can expect to see a maximum in the energy-sharing distribution of the correlated pairs in the intersection region. This maximum will correspond to single scattering of the specularly reflected primary electron by the valence one in accordance with the chosen experimental parameters. We can compare experimental energy-sharing distributions (Fig. 5) with the result of free-electron-like model predictions (Fig. 7). It turns out that in both cases we see one maximum in the energy-sharing curve. The energy of this maximum is $\pm 7$ eV (the sign depends on the experimental geometry), and the calculated position of this maximum ($\pm 10$ eV) is slightly higher than the measured one. Thus, we see qualitative agreement between the experimental result and the simple model prediction. This suggests that the most probable location of the pairs in the two-dimensional energy distribution reflects the conditions in which the experimental trace in $k$-space crosses the equi-energy shell of the valence electron states corresponding to a certain binding energy.

In general, correlated electron pairs can be excited either by diffracted incident electrons or by isotropically scattered ones. For normal incidence in both cases the energy sharing distributions will be symmetric because the sample is a cubic crystal and the detectors are in symmetric positions with respect to the surface normal. This means that in this geometry the two electron detectors are indistinguishable and this is the reason for the symmetric energy-sharing distribution. For the off-normal incidence, an isotropic elastic scattering model for the primary electrons gives an isotropic angular distribution of elastically scattered electrons for any incident angle. In this case the energy-sharing distribution of correlated pairs would again be symmetric because an isotropic scattering of incident electrons keeps the full symmetry of the (e,2e) process.

On the other hand the incident electron beam can undergo diffraction and then diffracted electrons can generate correlated electron pairs. In this case the energy-sharing distributions may be either symmetric or asymmetric, depending on the direction of the diffracted beam (beams).

The measured asymmetry in the energy sharing distribution within correlated pairs for off-normal incidence (Fig. 5) indicates that they are generated in asymmetric kinematics. The analysis of this kinematics shows that correlated pairs are mostly created by specularly reflected electrons. Thus, the momentum conservation law for the (e,2e) process (2) in reflection kinematics can be rewritten as follows:

$$k_v = k_1 + k_2 - K_0\,, \tag{11}$$

where $k_v$ is the crystal momentum of the target electron, $k_1$ and $k_2$ are momenta of outgoing correlated electrons, $K_0 = k_0 - 2k_{on} + g$ is momentum of the diffracted incident electron, $k_{on}$ is the normal component of the incident electron momentum $k_0$, and $g$ is a reciprocal vector of the crystal lattice.

In Fig. 5 correlated pairs with $E_{tot} = 15 \pm 0.25$ eV are created in a single electron-electron collision because this is the highest possible total energy of the pair. Any additional electron-electron scattering is accompanied by an energy loss and leads to a decrease of the total energy of the pair. The energy-sharing distribution for this total energy indicates that they are generated in an asymmetric (e,2e) process. Moreover, this asymmetry will occur only for pairs generated in a single-step electron-electron collision. This means that as far as the energy-sharing distribution for a total energy of pairs below the cut-off is asymmetric, these pairs are mostly created in single electron-electron collisions. By contrast, in Fig. 5 for $E_{tot} = 9 \pm 05$ eV, the correlated electron pair creation in a multi-step process is very probable and this produces a more symmetric energy-sharing distribution. This allows us to estimate the probing energy range of (e,2e) spectroscopy in reflection geometry in the low-energy range. If we look at the energy-sharing distributions for $E_{tot}$ in the range 11–15 eV (Fig. 5), it can be seen that these distributions are asymmetric. It means that correlated pairs at these total energies are mostly created by the (e,2e) process in the same kinematic conditions as considered above and this shows a minor contribution of multi-step scattering in this energy range. It turns out that the energy range probed by the (e,2e) experiment in the present geometry is about 4 eV below the Fermi level.

## 4 Conclusions

In the present work we found that the energy distribution of correlated electron pairs excited by 20 eV primary electrons from W(001) depends on the kinematics of the (e,2e) process in the reflection geometry. For normal incidence and symmetric detector positions, the energy-sharing distributions of correlated electrons are symmetric. On the other hand, for off-normal incidence as well as for grazing incidence the energy-sharing distributions are asymmetric for correlated pairs excited from energy levels between the Fermi level and 4 eV below the Fermi level.

In the case of a cubic crystal, the symmetry of the energy-sharing distributions depends mostly on the geometry of experiment. Most of the correlated pairs from W(100) are created by specularly reflected or diffracted primary electrons. An asymmetry of the energy-sharing distributions appears when the specularly reflected electron beam has a certain angle with the surface normal.

Any point on the energy axis of the energy-sharing distribution corresponds to an electron state in the scattering plane of the $k$-space of valence electrons. The energy axis corresponds to the scanning trace in the scattering plane of the $k$-space and defines detectable electron states. The position of the maximum in the energy-sharing distribution reflects the intersection of the scanning trace with the equi-energy contour in the scattering plane. Thus, the maximum position defines an electron state in the $k$-space of valence electrons.

The present work clearly shows that under our experimental conditions correlated electron pairs are created mostly by incident electrons diffracted on the crystal lattice of the solid. This makes the (e,2e) experiment in the reflection geometry kinematically well defined. The minor contribution of multi-step electron-electron collisions in the energy band of a few electron volts below the Fermi edge shows that (e,2e) experiments in the reflection geometry may be considered as a useful tool for studying the electronic structure of solids and the scattering dynamics of low-energy electrons in the surface region.

*Acknowledgements.* We thank H. Schwabe for his design and preparation of the detection system and H. Engelhard for his technical assistance.

## References

1. V.G. Levin, V.G. Neudachin, Yu.F. Smirnov: Phys. Stat. Sol. (b) **49**, 489 (1972)
2. A. D'Andrea, R. Del Sole: Surf. Sci. **71**, 306 (1978)
3. M. Vos, I.E. McCarthy: Rev. Mod. Phys. **67**, 713 (1995)
4. Y.Q. Cai, M. Vos, P. Storer, A.S. Kheifets, I.E. McCarthy, E. Weigold: Solid State Commun. **95**, 25 (1995)
5. C. Gao, A.L. Ritter, J.R. Dennison, N.A.W. Holzwarth: Phys. Rev. B **37**, 3914 (1988)
6. P. Hayes, M.A. Bennett, J. Flexman, J.F. Williams: Phys. Rev. B **38**, 13371 (1988)
7. J. Kirschner, O.M. Artamonov, A.N. Terekhov: Phys. Rev. Lett. **69** (1992)
8. O.M. Artamonov, S.N. Samarin, J. Kirschner: Phys. Rev. B **51** (1995)
9. J. Kirschner, O.M. Artamonov, S.N. Samarin: Phys. Rev. Lett. **75** (1995)
10. S. Iacobucci, L. Marassi, R. Camilloni, S. Nannarone, G. Stefani: Phys. Rev. B **51**, 10252 (1995)